

A characterization of the diffuse Galactic emissions in the anti-center of the Galaxy

L. Fauvet^{1,2}, J. F. Macías-Pérez², S. R. Hildebrandt^{2,3}, F.-X. Désert⁴

(1) European Space Agency (ESA), Research and Scientific Support Dpt., Astrophysics Division, Keplerlaan 1, 2201AZ Noordwijk, The Netherlands

(2) LPSC, Université Joseph Fourier Grenoble 1, CNRS/IN2P3, Institut National Polytechnique de Grenoble, 53 avenue des Martyrs, 38026 Grenoble cedex, France

(3) California Institute of Technology, 1200 E. California Blvd., 91125 Pasadena, USA

(4) Laboratoire d'astrophysique de Grenoble, IPAG, Université Joseph Fourier BP 53, 38041 Grenoble CEDEX 9, France

Abstract—Using the Archeops and WMAP data we perform a study of the anti-center Galactic diffuse emissions – thermal dust, synchrotron, free-free and anomalous emission – at degree scales. The high frequency data are used to infer the thermal dust electromagnetic spectrum and spatial distribution allowing us to precisely subtract this component at lower frequencies. After subtraction of the thermal dust component a mixture of standard synchrotron and free-free emissions does not account for the residuals at these low frequencies. Including the all-sky 408 MHz Haslam data we find evidences for anomalous emission with a spectral index of -2.5 in T_{RJ} units. However, we are not able to conclude regarding the nature of this anomalous emission in this region. For the purpose, data between 408 MHz and 20 GHz covering the same sky region are needed.

Index Terms—ISM: general – ISM: clouds – Methods: data analysis – Cosmology: observations – Submillimeter – Catalogs

I. INTRODUCTION

The anomalous microwave emission (AME in the following), is an important contributor of the Galactic diffuse emissions in the range from 20 to 60 GHz. It was first observed by (de Oliveira-Costa et al., 1997; Kogut et al., 1996) and then identified by (Leitch et al., 1997) as free-free emission from electrons with temperature, $T_e > 10^6$ K. Draine & Lazarian (1998a) argued that AME may result from electric dipole radiation due to small rotating grains, the so-called *spinning dust*. Models of the *spinning dust* emission (Draine & Lazarian, 1998b) show an electromagnetic spectra peaking at around 20-50 GHz being able to reproduce the observations (Finkbeiner, 2003; de Oliveira-Costa et al., 2004; Watson et al., 2005; Iglesias-Groth, 2005; Casassus et al., 2006, 2008; Dickinson et al., 2009; Tibbs et al., 2010). The initial *spinning dust* model has been refined regarding the shape and rotational properties of the dust grains (Ali-Haïmoud et al., 2009; Hoang et al., 2010, 2011; Silsbee et al., 2011). An alternative explanations of AME was proposed by Draine & Lazarian (1999) based on magnetic dipole radiation arising from hot ferromagnetic grains. This kind of models associated to single-domain predict polarization fraction much bigger than the electric dipole ones (Lazarian & Draine, 2000). Original models have been mainly ruled out by many studies (Battistelli et al., 2006; Casassus et al., 2006; Kogut, 2007; Mason et al., 2009; López-Caraballo et al., 2011) although modern variants of those

may still be of interest (B. Draine private communication).

Correlation between microwave and infrared maps, mainly dominated by dust thermal emission (Désert et al., 1990), was observed for various experiments, for example on COBE/DMR (Kogut et al., 1996a,b), OVRO (Leitch et al., 1997), Saskatoon (de Oliveira-Costa et al., 1997), survey at 19GHz (de Oliveira-Costa et al., 1998), Tenerife (de Oliveira-Costa et al., 1999). Similar signal was find in small region by (Finkbeiner, 2003) and in some molecular clouds based on data from COSMOSOMAS (Génova-Santos et al., 2011; Watson et al., 2005), AMI (Ami-Consortium: Scaife et al., 2009a,b), CBI (Casassus et al., 2006; Castellanos et al., 2011), VSA (Tibbs et al., 2010) and Planck (Planck-Collaboration, 2011). Recent studies based on several sets of data (Bot et al., 2010) found similar results.

Independently, Bennett et al. (2003) proposed an alternative explanation of AME based on flat-spectrum synchrotron emission associated to star-forming regions to explain part of the WMAP first-year observations. This hypothesis seems to be disagreement with results from de Oliveira-Costa et al. (2004); Fernández-Cerezo et al. (2006); Hildebrandt et al. (2007); Ysard et al. (2010) which showed that spinning dust was the most trustable emission to explain the excess below 20 GHz. Furthermore, Davies et al. (2006) showed the existence of important correlation between microwave and infrared emission in regions outside star-forming areas. More recently, Kogut et al. (2011) discussed the fact that *spinning dust* fits better to ARCADE data (3.8 and 10 GHz) than a flat-spectrum synchrotron.

We propose here to study the Galactic diffuse emissions in the Galactic plane, particularly focusing on the anti-center region. The observational data, from 408 MHz to 3000 GHz, used for this study are presented in Section II. Section III discusses in details the contribution of the diffuse Galactic thermal dust emission using the high frequency data. In Section IV we consider a simple free-free and canonical synchrotron emission model for the thermal dust subtracted microwave data. The possible contribution from anomalous emission is discussed in Section V. We draw conclusions in Section VI.

II. MICROWAVE AND MILLIMETER OBSERVATIONS

We describe in this section the data used for the analysis presented in this paper. As we are interested in the Galactic diffuse emission we consider only large coverage sky surveys in the radio, microwave, millimeter and infrared domain including the 408 MHz all-sky survey and the WMAP ARCHEOPS and IRAS data.

408 MHz all-sky survey

In the radio domain, the 408MHz all-sky continuum survey (Haslam et al. (1982)) at a resolution of of 0.85 degrees, is a good tracer of the synchrotron emission. In particular, we use

TABLE I
RMS OF THE HIGH FREQUENCY DATA AND OF THE RESIDUALS AFTER SUBTRACTION OF THE DUST MODEL.

Frequency (GHz)	Data rms (mK _{RJ})	Residual rms (mK _{RJ})	Noise standard deviation (mK _{RJ})
143	0.194407	0.0240274	0.0241575
217	0.315175	0.0306455	0.0406982
353	0.498923	0.0705655	0.0404479
545	0.699145	0.113738	0.157994
3000	0.0973817	0.00830546	0.0197808
5000	0.0134645	0.00974734	0.00176314

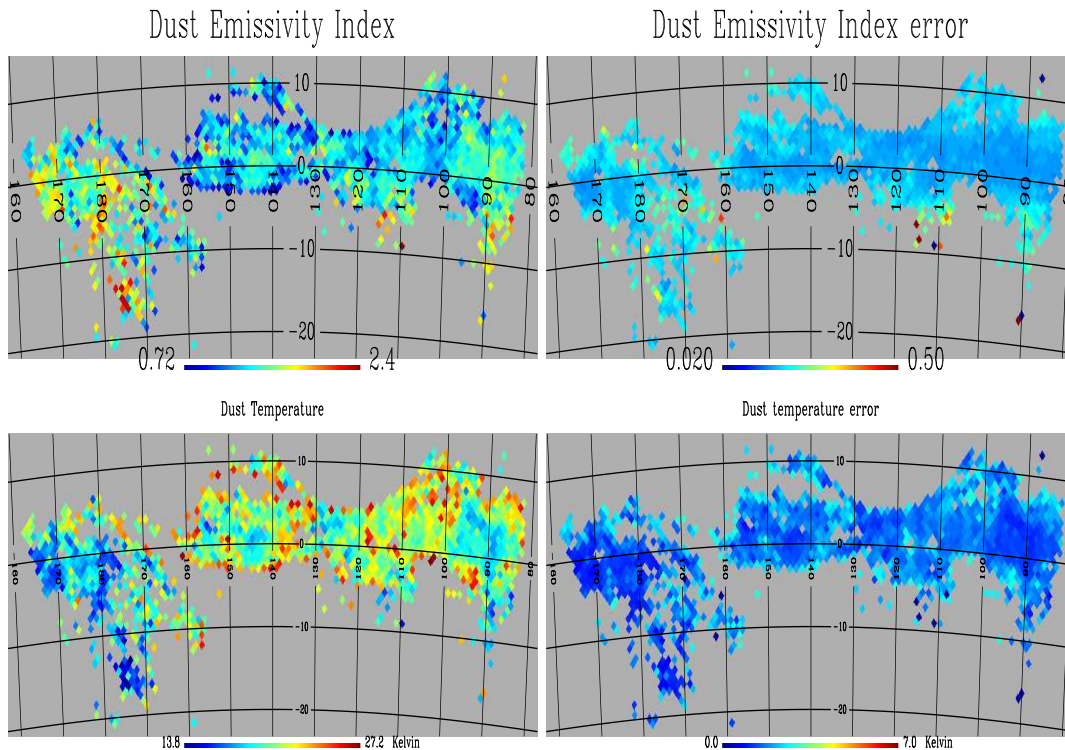


Fig. 1. From top to bottom and from left to right: maps of the best-fit thermal dust emission spectral indices and temperature and uncertainties at 2σ (95 % C.L.) (right).

the 408MHz all-sky map available on the LAMBDA website in the HEALPIX pixelisation scheme (Górski et al., 2005). The 408 MHz all-sky survey map was smoothed down to a resolution of 1 degree and downgraded to $N_{side} = 64$ in the HEALPIX pixelisation scheme (Górski et al. (2005)). The uncertainties on this map are assumed to be of 10 % following Haslam et al. (1982) and are mainly due to calibration errors.

WMAP

In order to estimate the diffuse Galactic emission at microwave frequencies we used the maps in temperature using the K, Ka, Q, V and W band maps of the WMAP mission of its 7-years WMAP citephinsaw09. In particular, we used the co-added maps available on the the Lambda web site, also smoothed down to a resolution of 1 degree and downgraded to $N_{side} = 64$. Uncertainties in the WMAP data were computed assuming a uncorrelated anisotropic noise as described in (Hinshaw et al., 2009). The variance per pixel at the working resolution was computed using the variance of a single hit and the number of hits per pixels.

ARCHEOPS

In the millimeter wavelengths we use the ARCHEOPS balloon experiment (Benoît et al., 2004) data. ARCHEOPS ob-

served the sky at four frequency bands: 143, 217, 353 and 545 GHz, with a resolution of 11, 13, 12 and 18 arcmin respectively (Macías-Pérez et al., 2007). The ARCHEOPS survey covers about 30 % of the sky mainly centered in the Galactic anti-center region. We use here the original ARCHEOPS maps which were also smoothed down to a resolution of one degree and downgraded to $N_{side} = 64$.

IRAS

In the infrared, we have used the new generation of the IRAS data (*InfraRed Astronomical Satellite*) at 100 and 60 μm (3000 and 5000 GHz). This release of the IRAS data is called IRIS (*Improved Reprocessing of the IRAS data*) (Miville-Deschênes, 2005) and has been built with a better destroying, a better subtraction of the zodiacal light and a calibration and a zero level compatible with the far infrared instrument, FIRAS, of COBE. The IRIS maps were also smoothed down to a resolution of one degree and downgraded to $N_{side} = 64$.

In order to avoid the contamination from the CMB at intermediate frequencies, 30-200 GHz, we have restricted our study to the Galactic plane where the Galactic emissions dominate over the cosmological CMB emission. In practice, we selected those regions in the Archeops 353 GHz map with intensity above 3000

TABLE II

RANGE OF VALUES CONSIDERED FOR THE PARAMETERS OF THE THERMAL DUST EMISSIVITY MODEL.

Parameters	Range	Step
β_d	[-1.0, 4.0]	0.02
T_d	[10.0, 37.0]	0.1

μK_{RJ} or higher. This corresponds to 1391 pixels at $N_{side} = 64$ in the anticenter region.

III. DIFFUSE GALACTIC THERMAL DUST EMISSION

We first study the electromagnetic and spatial properties of the thermal dust diffuse Galactic emission. In order to model the intensity of the thermal dust emission, we use a simple grey body spectrum of the form

$$I_\nu = I_0 \nu^{\beta_d} B_\nu(T_d) \quad (1)$$

where β_d is the spectral index of the thermal dust emission and T_d is the dust temperature.

We used the ARCHEOPS and IRIS 100 μm maps to characterize the dust thermal emission model. We fitted the data to the model pixel by pixel using as free parameters I_0 , β_d and T_d , and the following likelihood function

$$-\log \mathcal{L}_\nu = \sum_p \frac{(D_\nu^p - M_\nu^p)^2}{\sigma_\nu^2} \quad (2)$$

where D_ν^p and M_ν^p correspond to the data and model at the pixel p within the mask and for the observation frequency ν ($= 143, 217, 353, 545$ and 3000 GHz). σ_ν^p is the 1- σ error bar associated to D_ν^p . β_d and T_d were explored using a uniformly spaced grid as defined in Table II) while I_0 was computed via a linear fit for each pair (β_d, T_d) . The instrumental noise in the ARCHEOPS maps has been estimated using simulations of the noise in the ARCHEOPS Time Ordered Information (TOI) following the method described in Macías-Pérez et al. (2007). The variance per pixel was calculated from 250 simulated noise maps at one degree resolution and $N_{side} = 64$. The error bars for the IRIS data at 100 μm were set to 13.5 % following (Miville-Deschênes, 2005) as they are dominated by calibration errors.

In Figure 1 we present maps of the dust temperature and spectral index within the considered mask. We also show the statistical uncertainties on these parameters. As expected the errors increase significantly on the edges of the maps. These noisy pixels will be excluded from the analysis hereafter. We can also notice that in the inner regions the statistical errors are significantly smaller than the observed dispersion for the two parameters. We observe that the mean dust temperature is 20.0 K with 2.1 K dispersion, while the mean instrumental uncertainties are of the order of 1 K. In the same way, the mean dust spectral index is 1.40 with a dispersion of 0.25, and the mean instrumental uncertainties of the order of 0.1.

Figures ?? and 2 compare the best-fit thermal dust model to the IRAS and ARCHEOPS data. From left to right we show the data, the model and residuals for all frequencies. For the ARCHEOPS data the residuals are at most 10 % of the total intensity. In the case of the IRAS data the model reproduce rather well the 100 μm map. However, at 60 μm , the residuals are important and the model is not able reproduce the structure in the data. Residuals can be as important as 60 % of the total intensity. This can be explained by the presence of a hotter dust component as discussed in Désert et al. (1990). This component is out of the

TABLE III

SPECTRAL INDEX OF THE FREE-FREE EMISSION AT THE WMAP FREQUENCIES ASSUMING AN ELECTRONIC TEMPERATURE OF $T_e=8000$ K.

central frequency (GHz)	23	33	41	61	94
β_{ff}	-2.090	-2.093	-2.095	-2.099	-2.103

TABLE IV

RANGE OF THE PARAMETERS CONSIDERED FOR THE ANOMALOUS AND FREE-FREE EMISSION MODELS.

Parameters	Ranges	Step
β_s	[-3.7, -2.3]	0.01
T_e (K)	[4000.0, 14000]	1000

scope of this study and does not have any consequence in the following study. Table I presents the rms of the ARCHEOPS and IRAS data as well as the rms of the residuals after subtraction of the dust model. The last column of the table represents the mean standard deviation of the noise in the original maps. We observe that except for the 5000 GHz data the residuals are of the order of magnitude of the noise.

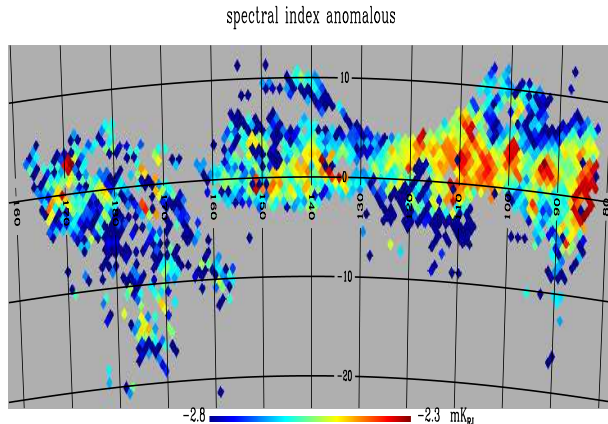


Fig. 4. Map of the spectral index of the anomalous emission. (right).

IV. DIFFUSE GALACTIC FREE-FREE AND SYNCHROTRON EMISSIONS

In order to estimate the contribution of the diffuse galactic free-free emission, which is expected to be important at the WMAP bands, we use the *Extinction-Corrected H α Foreground Template* (H α) map built by Finkbeiner (2003). This map was computed using data from the *Virginia Tech Spectral line Survey* (VTSS), for the North and of data from the *Southern H-Alpha Sky Survey Atlas* (SHASSA) for the South sky. Correction factors are applied to take into account dust absorption (Finkbeiner, 2003). We started from a map at resolution $N_{side} = 512$ and downgraded it, as the other maps, at a resolution of $N_{side} = 64$. In order to obtain a template of the free-free emission at 23 GHz using the H α map, we follow Bennett et al. (2003). In antenna temperature units and defining the emission measure as $EM = \int n_e^2 dn$, one can write

$$T_A^{ff}(\mu K) = 1.44 EM_{cm^{-6}.pc} \frac{[1 + 0.22 \ln(T_e/8000K) - 0.14 \ln(\nu/41GHz)]}{(\nu/41GHz)^2 (T_e/8000K)^{1/2}} \quad (3)$$

The intensity of the H α $I(R)$ emission (in Rayleigh units) is defined by

$$I(R) = 0.44EM_{cm}^{-6.pc} \left(\frac{T_e}{8000K} \right)^{-1/2} \times \left(1 - 0.34 \ln \left(\frac{T_e}{8000K} \right) \right) \quad (4)$$

Thus the intensity of the free-free emission (in mK_{RJ}) is given as a function of the intensity of the $H\text{-}\alpha$ emission (in Rayleighs) by

$$T_{ff} = \frac{1.44}{0.44} I(R) \frac{\left(1 + 0.22 \ln \left(\frac{T_e}{8000K} \right) - 0.14 \ln \left(\frac{\nu}{41GHz} \right) \right)}{\left(\frac{\nu}{41GHz} \right)^2 \left(1 - 0.34 \ln \left(\frac{T_e}{8000K} \right) \right)} \quad (5)$$

We have extrapolated this free-free emission template at each of the WMAP frequencies assuming that the electromagnetic spectrum of the free-free emission is well represented by a power law of the form $\nu^{\beta_{ff}}$ (Bennett et al., 2003)

$$\beta_{ff} = -2 - \frac{1}{10.48 + 1.5 \ln(T_e/8000K) - \ln(\frac{\nu}{41GHz})} \quad (6)$$

We set a standard value for the electronic temperature at 8000 K, following (Otte et al., 2002). The values of the spectral index obtained at the WMAP frequencies assuming these hypothesis are given in Table III.

In order to model the synchrotron contribution we used the *408 MHz all-sky continuum survey* as a template map. We extrapolated it at all the considered frequencies assuming a power law like electromagnetic spectrum in antenna temperature with fix spectral index that we set to -2.7 (Bennett et al., 2003).

In the second column of Table ?? we present the rms of the residuals after subtraction of the Galactic thermal dust, synchrotron and free-free emission models. These residuals are significant: up to 90 % of the original emission (first column of the table). We have observed both point like and diffuse structures in these residuals. The former are more probably related to uncertainties in the modeling of the free-free emission. By contrast, the extra diffuse emission is most probably related to anomalous emission. This hypothesis is considered in the following section.

V. STUDY OF THE ANOMALOUS EMISSION

In the previous section we concluded that the observed emission in the range from 23 to 94 GHz can not be explained only by the combination of the canonical Galactic diffuse emission: thermal dust, soft synchrotron and free-free. Indeed, we have observed that in some compact regions there seems to be extra free-free emission with respect to the predictions from the $H\alpha$ template . Furthermore, the diffuse emission is underestimated in general indicating either an extra component or a softer synchrotron component. In order to investigate these two problems we have considered a two component model composed of free-free and anomalous emissions in addition to diffuse thermal dust emission. We assume that the free-free and the anomalous emissions follow a simple power-law model such that

$$M_\nu = A_{anom} \nu^{\beta_{anom}} + A_{ff} \nu^{\beta_{ff}(T_e, \nu)} \quad (7)$$

where M_ν are the observed maps in K_{RJ} units at the frequency ν after subtraction of the contribution from thermal dust. Finally, we consider 4 free parameters in the model: the normalization coefficients A_{sync} and A_{ff} , the spectral index β_s of the anomalous component and the free electron temperature (??). To simplify the fitting procedures we vary β_s and T_e in the ranges shown in Table IV. Notice that we have not explicitly consider the canonical synchrotron emission in this model. Indeed, our so

called anomalous component will be a mixture of real anomalous emission and canonical synchrotron emission.

We fit this two-component model to the dust subtracted WMAP maps and to the 408 MHz map for which the thermal dust emission is negligible. As discussed before, the uncertainties on the WMAP data have been calculated assuming anisotropic white noise on the maps. We compute the variance r pixel using the variance per single observation provided on the LAMBDA website and maps of the number of hit counts. For the 408 MHz map we assume 10 % uncertainties as discussed in Section II. It is important to notice that an alternative three component model (including free-free, canonical synchrotron and anomalous emission) would imply at least 6 free parameters to be fitted on only 6 sky maps. That is why we have chosen to consider a two-component model only.

From the results of the fit we observe that the anomalous emission seems to dominate the diffuse component at 1 GHz while the free-free emission seems to be mainly located in few compact regions. In Figure 4 we present the map of the reconstructed spectral index for the anomalous emission, β_s . We observe that the anomalous emission seems to be well represented by a power-law with average spectra index of -2.5. Similar results have been found by Bennett et al. (2003); Hinshaw et al. (2007) who claim conclusive evidence for hard synchrotron emission. In our analysis we did not dispose of data in the frequency range from 10 to 20 GHz to discriminate between this hypothesis and spinning dust emission (refer to Draine & Lazarian (1998a) for a more complete review on spinning dust emission). It is important to notice that currently spinning dust emission has mainly being found in particular Galactic clouds (see for example de Oliveira-Costa et al. (1999, 2002); Lagache (2003); Hildebrandt et al. (2007); Watson et al. (2005); Ysard et al. (2010); Dickinson et al. (2010); Bot et al. (2010); Planck Collaboration et al. (2011c)). Regarding the electron temperature, we have found that a physically accessible temperature is associated to only 40 out of 1039 pixels considered. These pixels corresponds to the intense regions on the free-free map at 1 GHz. For the other pixels, the temperature is higher than the upper limit allowed (Otte et al., 2002) and then can not be linked to the free-free emission.

VI. SUMMARY AND CONCLUSIONS

We have presented in this paper a detailed analysis of the Galactic diffuse emissions at the Galactic anti center in the frequency range from 23 to 545 GHz. We have shown that a simple grey-body model can be used to describe the thermal dust emission in the frequency range from 100 to 3000 GHz. We find a mean temperature of 20 K with an intrinsic dispersion of 2.1 K and a spectral index of 1.4 with intrinsic dispersion of 0.25. These values are significantly larger and lower than expected from canonical models of the dust emission, $T_{dust} \sim 17$ K and $\beta_{dust} = 1.8 - 2$ (see for example Finkbeiner et al. (1999); Planck Collaboration et al. (2011a)). The same kind of results have been found by Planck Collaboration et al. (2011b), although as they fixed the spectral index to 1.8 they obtain a lower temperature of 14 K. We have performed a similar analysis fixing $\beta_{dust} = 1.8$ and we have also obtained lower dust temperatures. At high frequencies (above 3000 GHz) extra hot thermal dust emission from small dust grains is needed to account for the observations (Désert et al., 1990).

The former dust model have been used to extrapolate the thermal dust emission to microwave frequencies from 23 to 100 GHz. After subtraction of the thermal dust emission we have shown that the microwave data can not be simply explained by a combination of free-free and canonical synchrotron emission. A more detailed analysis including AME has shown that the latter can be well approximated by a power-law of average spectral

TABLE V

RMS OF THE WMAP DATA AND OF THE RESIDUALS AFTER SUBTRACTION OF THE DUST, FREE-FREE AND STANDARD SYNCHROTRON MODEL AND OF THE DUST, FREE-FREE AND ANOMALOUS EMISSION MODEL COMPARED TO THE STANDARD DEVIATION OF THE NOISE.

Frequency (GHz)	Data rms (mK _{RJ})	Residual DFS rms (mK _{RJ})	Residual DFA rms (mK _{RJ})	Noise standard deviation (mK _{RJ})
23	2.03831	2.02387	0.353262	0.183557
33	0.907433	0.884012	0.0881647	0.0612279
41	0.562764	0.531677	0.0372230	0.0438113
61	0.256907	0.205086	0.0377750	0.0205909
94	0.209367	0.112932	0.0530679	0.0239733

index -2.5 in K_{RJ} units. This anomalous emission seems to dominate the diffuse emission at microwave frequencies while free-free emission seems to be located in few compact regions. Indeed, we have found that outside those regions the data required electron temperature has not physically meaningful.

The spectral index found for the anomalous emission is consistent with hard synchrotron emission (Bennett et al., 2003; Hinshaw et al., 2007). However, we can not formally conclude on this as our analysis did not include data in the 1 to 20 GHz that would help discriminating this hypothesis from spinning dust emission Draine & Lazarian (1998a) for which conclusive evidence have been found on some Galactic clouds de Oliveira-Costa et al. (1999, 2002); Lagache (2003); Watson et al. (2005); Ysard et al. (2010); Dickinson et al. (2010); Bot et al. (2010); Planck Collaboration et al. (2011c) and as diffuse emission by Hildebrandt et al. (2007).

ACKNOWLEDGEMENTS

The authors would like to thanks R. Davies and C. Dickinson for useful discussions. SH would like to thank the LPSC and, especially, Dr. Juan Macias and Prof. Daniel Santos for the time he spent at LPSC during 2010.

REFERENCES

- Ali-Haïmoud, Y., Hirata, C. M., & Dickinson, C. 2009, MNRAS, 395, 1055
- Ami-Consortium: Scaife, A. M. M., Hurley-Walker, N., & Green, D. A. 2009a, MNRAS, 394, 46
- Ami-Consortium: Scaife, A. M. M., Hurley-Walker, N., & Green, D. A. 2009b, MNRAS, 400, 1394
- Battistelli, E. S., Rebolo, R., & Rubiño Martín, J. 2006, ApJ, 645, 141
- Bennett, C., Halpern, M., Hinshaw, G., et al. 2003, ApJs, 148, 1
- Benôit, A., Ade, P., Amblard, A., et al. 2004, A & A, 424, 571
- Bot, C., Ysard, N., Paradis, D., et al. 2010, A&A, 532, 20
- Casassus, S., Cabrera, G. F., & Förster. 2006, ApJ, 639, 951
- Casassus, S., Dickinson, C., & Cleary, K. 2008, MNRAS, 391, 1075
- Castellanos, P., Casassus, S., & Dickinson, S. 2011, MNRAS, 411, 1137
- Davies, R. D., Dickinson, C., & Banday, A. 2006, MNRAS, 370, 1125
- de Oliveira-Costa, A., Kogut, A., & Devlin, M. J. 1997, ApJ, 482, 17
- de Oliveira-Costa, A., Kogut, A., Devlin, M. J., et al. 1997, ApJL, 482, L17
- de Oliveira-Costa, A., Tegmark, M., & Davies, R. D. 2004, ApJ, 606, 89
- de Oliveira-Costa, A., Tegmark, M., Finkbeiner, D. P., et al. 2002, ApJ, 567, 363
- de Oliveira-Costa, A., Tegmark, M., Gutierrez, C. M., et al. 1999, ApJ, 527, 9
- de Oliveira-Costa, A., Tegmark, M., Page, L. A., & Boughn, S. P. 1998, ApJ, 509, 9
- Désert, F.-X., Boulanger, F., & Puget, J. 1990, A & A, 237, 215
- Dickinson, C., Casassus, S., Davies, R., et al. 2010, MNRAS, 407, 2223
- Dickinson, C., Davies, R. D., & Allison, J. R. 2009, ApJ, 690, 1585
- Draine, B. & Lazarian, A. 1998a, ApJ, 494, 19
- Draine, B. & Lazarian, A. 1998b, ApJ, 508, 57
- Draine, B. T. & Lazarian, A. 1999, ApJ, 512, 740
- Fernández-Cerezo, S., Gutiérrez, C. M., & Rebolo, R. 2006, MNRAS, 370, 15
- Finkbeiner, D. P. 2003, ApJ, 146, 407
- Finkbeiner, D. P., Davis, M., & Schlegel, D. J. 1999, ApJ, 524, 867
- Génova-Santos, R., Rebolo, R., Rubiño Martín, J., C. H. López-Caraballo, C., & Hildebrandt, S. 2011, ApJ, 743, 1
- Górski, K., Hivon, E., Banday, A., et al. 2005, ApJ, 622, 759
- Haslam, C., Salter, C., Stoffel, H., & Wilson, W. E. 1982, A&As, 47, 1
- Hildebrandt, S., Rebolo, R., Rubino-Martín, J. A., et al. 2007, MNRAS, 382, 594
- Hinshaw, G., Nolta, M., Bennett, C., et al. 2009, ApJs, 180, 225
- Hinshaw, G., Nolta, M. R., Bennett, C. L., et al. 2007, ApJs, 170, 288
- Hoang, T., Draine, B. T., & Lazarian, A. 2010, ApJ, 715, 1462
- Hoang, T., Lazarian, A., & Draine, B. T. 2011, ApJ, 741, 2
- Iglesias-Groth, S. 2005, ApJ, 632, 25
- Kogut, A., Banday, A. J., & Bennett, C. L. 1996a, ApJ, 460, 1
- Kogut, A., Banday, A. J., & Bennett, C. L. 1996b, ApJ, 464, 5
- Kogut, A., Banday, A. J., Bennett, C. L., et al. 1996, ApJL, 464, L5
- Kogut, A., Fixsen, D. J., & Levin, S. M. 2011, ApJ, 734, 4
- Kogut, A. e. a. 2007, ApJ, 665, 335
- Lagache, G. 2003, A & A, 405, 813
- Lazarian, A. & Draine, B. T. 2000, ApJ, 536, 15
- Leitch, E. M., Readhead, A. C. S., Pearson, T. J., & Myers, S. T. 1997, ApJ, 486, 23
- López-Caraballo, C., Rubiño Martín, J., Rebolo, R., & Génova-Santos, R. 2011, ApJ, 729, 25
- Macías-Pérez, J., Lagache, G., Maffei, B., et al. 2007, A&A, 467, 1313
- Mason, B. S., Robishaw, T., Heiles, C., Finkbeiner, D., & Dickinson, C. 2009, ApJ, 697, 1187
- Miville-Deschênes, M.-A. & Lagache, G. 2005, ApJs, 157, 302
- Otte, B., Gallagher, J., & Reynolds, R. J. 2002, ApJ, 572, 823
- Planck-Collaboration. 2011, A & A, 536, 20
- Planck Collaboration, Abergel, A., Ade, P. A. R., et al. 2011a, A&A, 536, A24
- Planck Collaboration, Ade, P. A. R., Aghanim, N., et al. 2011b, A&A, 536, A19
- Planck Collaboration, Ade, P. A. R., Aghanim, N., et al. 2011c, A&A, 536, A20
- Silsbee, K., Ali-Haïmoud, Y., & Hirata, C. M. 2011, MNRAS, 411, 2750
- Tibbs, C. T., Watson, R. A., & Dickinson, C. 2010, MNRAS, 402, 1969
- Watson, R., Rebolo, R., Rubino-Martín, J. A., et al. 2005, ApJ, 624, 89
- Ysard, N., Miville-Déschenes, M.-A., & Verstraete, L. 2010, A &

A, 509, 18

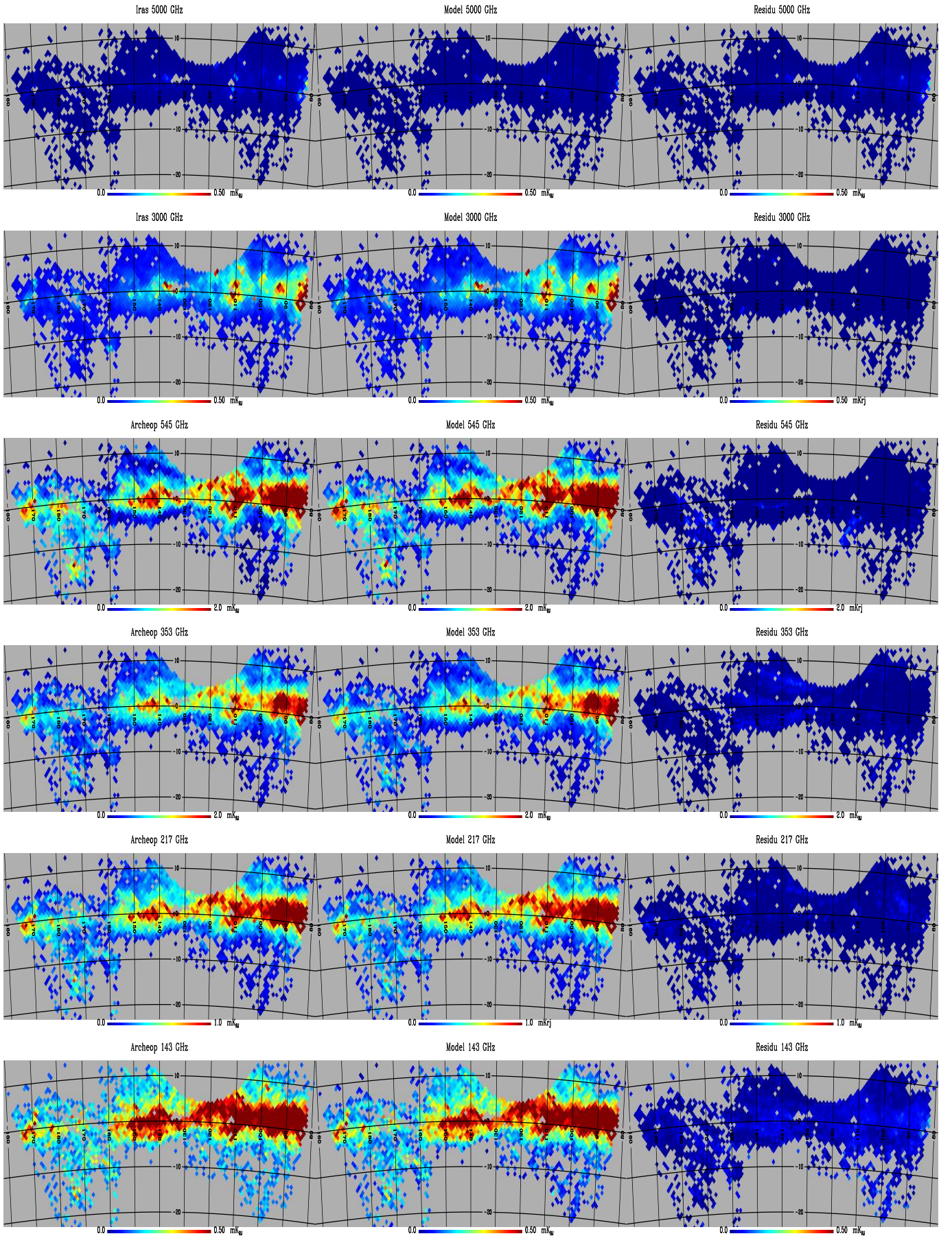


Fig. 2. Temperature maps (mK_{RJ}) for the ARCHEOPS data (*left*), the thermal dust emission model (*center*) and residuals (*right*). From top to bottom we present the 545, 353, 217 and 143 GHz maps.

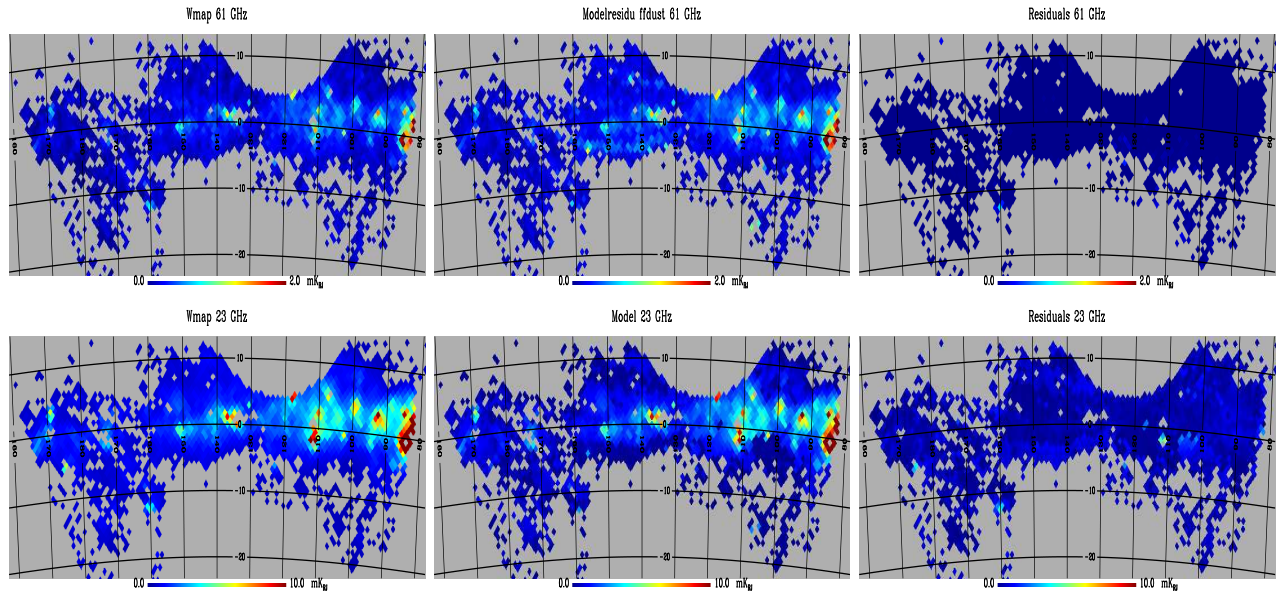


Fig. 3. From left to right: Residuals after subtraction of the thermal dust, free-free and anomalous emission models for the 61 (top) and 23 GHz (bottom) maps.